

This is a repository copy of *Heusler Alloys for Metal Spintronics*.

White Rose Research Online URL for this paper:

<https://eprints.whiterose.ac.uk/187184/>

Version: Published Version

Article:

Hirohata, Atsufumi orcid.org/0000-0001-9107-2330 and Lloyd, David (2022) Heusler Alloys for Metal Spintronics. MRS BULLETIN. 593–599. ISSN 0883-7694

<https://doi.org/10.1557/s43577-022-00350-1>

Reuse

This article is distributed under the terms of the Creative Commons Attribution (CC BY) licence. This licence allows you to distribute, remix, tweak, and build upon the work, even commercially, as long as you credit the authors for the original work. More information and the full terms of the licence here:

<https://creativecommons.org/licenses/>

Takedown

If you consider content in White Rose Research Online to be in breach of UK law, please notify us by emailing eprints@whiterose.ac.uk including the URL of the record and the reason for the withdrawal request.



Heusler alloys for metal spintronics

Atsufumi Hirohata* and David C. Lloyd

Heusler alloys have been theoretically predicted and experimentally demonstrated to be an ideal spin source due to their half-metallicity at room temperature. The half-metallicity also offers low Gilbert damping constants for fast magnetization reversal with low switching current density. These intrinsic properties can offer better operationability in spin-transfer-torque-based devices. In addition spin-orbit torque can be exerted using Heusler alloys for spin Hall and caloritronic effects. These properties can be precisely controlled by substituting the constituent elements in a Heusler alloy. We review the recent development on these spintronic devices and summarize their future perspectives.

Introduction to spintronics

Spintronics is one of the emerging fields in nanoelectronics as a post-Moore solution.^{1,2} Metal spintronics has been focusing on the importance of the atomically smooth interfaces by utilizing the device fabrication techniques developed for the Si-based complementary metal oxide semiconductor (CMOS) technology.³ In comparison with the semiconductor spintronics with up to a micrometer-long depletion layer at the edge and interfaces of the patterned devices, the metal spintronics can suffer from spin-dependent electron scattering due to atomic roughness,⁴ which may form edge magnetic domains for example. Additional small resistance in metal spintronics by over two orders of magnitude can be advantageous for sustainable development of nanoelectronic devices with non-volatility in data storage in the form of a magnetic moment in a ferromagnetic layer.

Spintronic devices can be categorized into two types based on the dominant interactions employed: (1) between electron spins and (2) spin-orbit interactions. As shown in **Figure 1**, the former type uses spin-transfer torque (STT), which is provided from a spin-polarized electron to the others. This torque was formulated by Slonczewski⁵ and Berger⁶ independently. STT can be described as proportional to the cross product of the unit vector of a magnetization and the change in an electrical current density. Because the magnitude of

STT can only be increased linearly up to the Walker breakdown, the efficiency of STT can be dependent on the spin polarization of the ferromagnetic material used to generate spin-polarized electrons. For the spin generation, a Heusler alloy has great potential due to the half-metallicity at room temperature (RT).⁷ The generated up- and/or down-spin electrons can be treated as two individual currents as originally proposed by Mott.⁸ This simple model can explain the magnetoresistive (MR) phenomena, such as giant magnetoresistance (GMR)^{10,11} and tunneling magnetoresistance (TMR).¹² The GMR and TMR junctions consist of two ferromagnetic layers sandwiching a nonmagnetic and insulating layer, respectively. The magnetization of one of the ferromagnets, a free layer, are switched by a magnetic field or spin torques to form parallel and antiparallel configurations to another one, a reference layer, achieving changes in their resistance due to spin scattering. These MR phenomena improved the signal-to-noise ratios in a reading head of a hard disk drive (HDD) and a magnetic sensor, and also used as a cell of a magnetic random-access memory (MRAM).³ The latest MRAM commercially available uses a STT-based perpendicularly magnetized cell, which has been used in an aeroplane, a motor-bike, and a life tracker due to the robustness under extreme conditions. STT has also been used for the displacement of a magnetic entity formed in a ferromagnetic nanowire (e.g., a

Atsufumi Hirohata, Department of Electronic Engineering, University of York, UK; atsufumi.hirohata@york.ac.uk
David C. Lloyd, Department of Electronic Engineering, University of York, UK; david.lloyd@york.ac.uk
*Corresponding author
doi:10.1557/s43577-022-00350-1

magnetic domain wall¹³ and a magnetic skyrmion)¹⁴ leading to a racetrack memory (see Heusler Antiskyrmions section in this special issue for details).

The second type of spintronic devices utilizes the spin-orbit interactions (SOI) as formulated by Dirac initially.¹⁵ SOI is used to predict spin imbalance generation in a paramagnetic metal by introducing an electrical charge current without the application of an external magnetic field, as known as the spin Hall effect.^{16,17} By introducing a spin current instead, a spin Hall voltage can also be generated without a magnetic field, resulting in the inverse spin Hall effect. This is induced by skew and side-jump scattering of conduction electrons at a finite angle for low impurity concentration and with a finite shift by high impurity concentration, respectively, by SOI and is theoretically equivalent to anomalous Hall effect in a ferromagnet. Experimental observation of the spin Hall effect was performed in GaAs using magneto-optical Kerr effect imaging.¹⁸ The macroscopic scattering angle due to the spin Hall effect can be measured as the spin Hall angle θ_{SH} . Because SOI is determined as the product of SOI constant, spin and orbital moments, θ_{SH} can be maximized by selecting a material with a large SOI constant, which is typically proportional to the spin Hall conductivity. The relationship between the charge and spin currents can be defined as (Spincurrent) = $\theta_{SH} \times$ (Chargecurrent). A large SOI constant can also modify the spin configuration in a neighboring ferromagnet via the Dzyaloshinskii-Moriya interaction (DMI).^{19,20} The spin Hall conductivity has been reported to be enhanced by the presence of the 4*d* and 5*d* electrons²¹ as well as the partially filled *f*-orbitals.²² Such interactions can

stabilize a magnetic quasi-particle, such as a magnetic skyrmion,²³ consisting of a vortex configuration of magnetic spins continuously rotating along the radius, tangential and onion-shape from the perpendicularly oriented core to the outer spins antiparallel to the core. The magnetic skyrmion can be used as a magnetic information bit in a racetrack memory because of the advantages in the size and critical current density. SOI also controls the spin-polarized carrier transport in a semiconductor as predicted by Datta and Das²⁴ as detailed in Semiconductor Spintronics in this special issue. SOI can exert spin-orbit torque (SOT), which can also switch a magnetization in a ferromagnet.²⁵ SOT is known to be more efficient and faster than STT by almost one order of magnitude, which can be implemented in the next-generation MRAM for the power reduction and fast operation.³

Spin-transfer torque

Magnetoresistance

A key measure for a STT-based device is a magnetoresistance (MR) resistance, for example, GMR and TMR ratios, which can be defined as

$$MR\ ratio = \frac{\Delta R}{R} = \frac{(R_{AP} - R_P)}{R_P}$$

Here, R_{AP} and R_P represent the resistance measured with the antiparallel and parallel configurations of the magnetizations of the two ferromagnetic layers sandwiching a non-magnetic or insulating layer in a GMR or TMR junction. The GMR junctions generally show less than 100% MR ratios at RT, but with low resistance-area products (*RA*, below 1 $\Omega \mu m^2$

for the reduction of power consumption to be competitive with major RAMs) due to their all-metallic nature as shown in **Figure 2**. To date, the maximum GMR ratio is reported to be 82% at RT with *RA* of 31 $m\Omega \cdot \mu m^2$ for $Co_2FeGa_{0.5}Ge_{0.5}$ (10)/NiAl (0.21)/Ag (5)/NiAl (0.21)/ $Co_2FeGa_{0.5}Ge_{0.5}$ (10) (thickness in nm),²⁶ where NiAl is used to improve lattice matching between the ferromagnetic $Co_2Fe(Ga_{0.5}Ge_{0.5})$ Heusler alloy layer and the nonmagnetic Ag spacer. The TMR junctions, on the other hand, show much

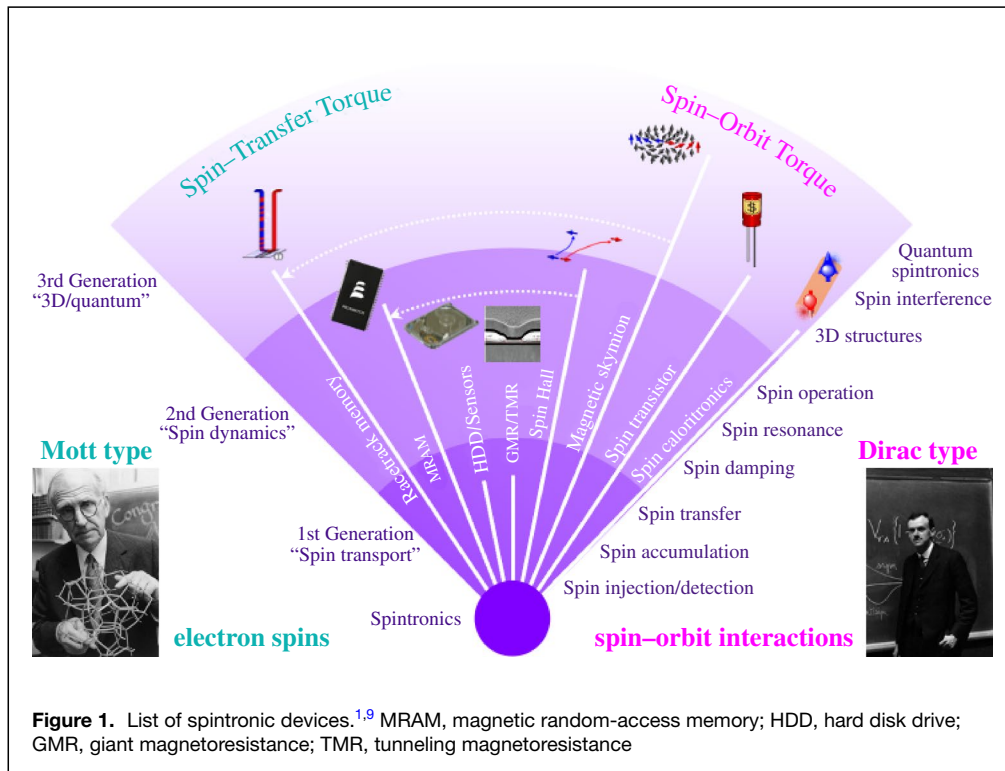


Figure 1. List of spintronic devices.^{1,9} MRAM, magnetic random-access memory; HDD, hard disk drive; GMR, giant magnetoresistance; TMR, tunneling magnetoresistance

larger MR ratios up to 604% at RT for a magnetic tunnel junction (MTJ) consisting of $\text{Co}_{0.2}\text{Fe}_{0.6}\text{B}_{0.2}$ (6)/MgO (2.1)/ $\text{Co}_{0.2}\text{Fe}_{0.6}\text{B}_{0.2}$ (4) (thickness in nm) at RT²⁷ using the Δ_1 -band matching between the ferromagnet and MgO layers for coherent tunneling as theoretically predicted,^{28,29} followed by experimental demonstration.^{30,31} For both junctions, further improvement in the MR junctions is necessary to satisfy the requirements for the set goals of 10 Gbit MRAM and 2 Tbit/in² HDD as shown in Figure 2. Recently perpendicularly magnetized CoFeB/MgO/CoFeB MTJs have successfully met the requirement for the 1 Gbit MRAM with RA of $18 \Omega \cdot \mu\text{m}^2$ and TMR ratio of 124% at RT.³²

For both GMR and TMR junctions, a half-metallic Heusler alloys should be able to achieve almost infinite MR ratios at RT. However, as shown in Figure 3a, the TMR ratios have not been increased over 10 years since the previously mentioned report with coherent tunneling.²⁷ Great efforts have been devoted using a half-metallic Heusler alloy film as a ferromagnetic layer in MTJs. The maximum TMR ratio is reported to be 342% at RT (616% at 4 K) with $RA = 2.5 \times 10^3 \Omega \cdot \mu\text{m}^2$ for epitaxial $B2\text{-Co}_2\text{FeAl}$ (5)/ $\text{Co}_{0.5}\text{Fe}_{0.5}$ (0.5)/ MgAl_2O_4 (1.2)/ $B2\text{-Co}_2\text{FeAl}$ (5) (thickness in nm).³³ Here, the MgAl_2O_4 tunneling barrier is used instead of MgO to improve the lattice matching of the junction with maintaining the coherent tunneling nature with the Δ_1 -band connection. By improving the quality of the Heusler alloy films by using $L2_1\text{-Co}_2\text{FeAl}_{0.5}\text{Si}_{0.5}$ in MTJ consisting of $L2_1\text{-Co}_2\text{FeAl}_{0.5}\text{Si}_{0.5}$ (30)/MgO (1.8)/ $L2_1\text{-Co}_2\text{FeAl}_{0.5}\text{Si}_{0.5}$ (5), the TMR ratios are reported to become 386% at RT (832% at 9 K) with $RA = 80 \times 10^3 \Omega \cdot \mu\text{m}^2$.³⁴ For polycrystalline sputtered full Heusler MTJs, on the other hand, much smaller TMR ratios have been reported due to the electron scattering at grain boundaries, for example, TMR of 175% at RT using a Co_2FeAl (2)/MgO (1.95)/ $\text{Co}_{0.75}\text{Fe}_{0.25}$ (5) (thickness in nm) structure,³⁵ confirming the quality of the Heusler alloy films and the interfacial smoothness in MTJs control the TMR ratios.

In these junctions, the decrease in the TMR ratio with increasing temperature is much faster than the temperature dependence of the magnetization as described by the empirical law of $T^{3/2}$. For example, for MTJ consisting of $L2_1\text{-Co}_2\text{MnSi}$ (3)/MgO (~ 2.5)/ $L2_1\text{-Co}_2\text{MnSi}$ (3) (thickness in nm), TMR ratio at 4 K is reported to be 1910% but that is reduced down to 354% at RT.³⁸ The steep reduction in the TMR ratio with increasing temperature below ~ 100 K is found to be a unique feature of the coherent tunneling as shown in Figure 3b. According to Shang's model,³⁹ the conductance for the parallel and antiparallel configurations, G_P and G_{AP} , respectively, at a finite temperature T can be described as

$$G_{P(AP)} = G_0(T) [1 + (-)P_0^2 m^2(T)] + G_{IS}(T), \quad 2$$

where G_0 is the mean conductance defined as $G_0(T) = G_0 CT / \sin CT$, P_0 is the tunneling spin polarization, m is the reduced magnetization due to the empirical law as $m(T) = AT^{3/2}$,⁴⁰ and G_{IS} is the spin-independent conductance due to the two-step hopping via defect states in a MgO barrier

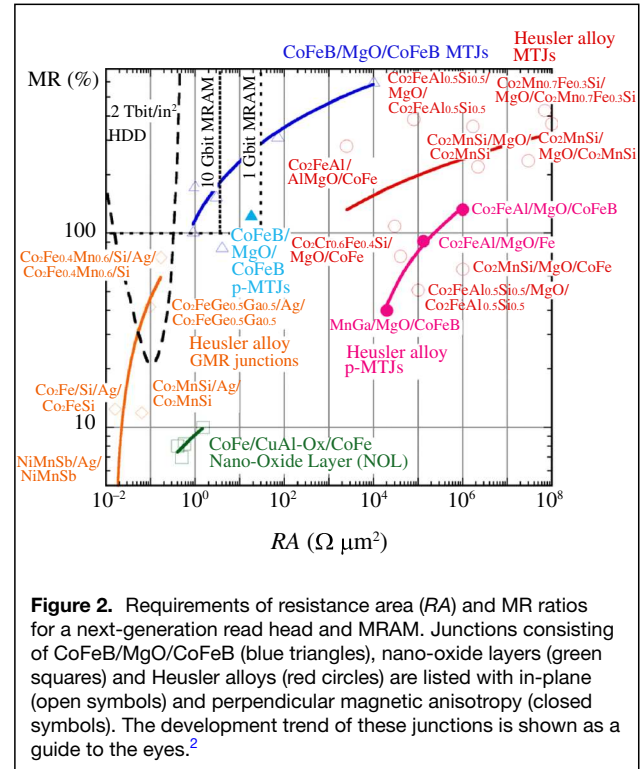


Figure 2. Requirements of resistance area (RA) and MR ratios for a next-generation read head and MRAM. Junctions consisting of CoFeB/MgO/CoFeB (blue triangles), nano-oxide layers (green squares) and Heusler alloys (red circles) are listed with in-plane (open symbols) and perpendicular magnetic anisotropy (closed symbols). The development trend of these junctions is shown as a guide to the eyes.²

expressed as $G_{IS}(T) = BT^4$. Here $C = 1.387 \times 10^{-3} d / \sqrt{\phi}$ with the barrier width d in nm and height ϕ in eV. G_0 and B are constants. A is the parameter characterizing spin fluctuation at the interface between a ferromagnet and a barrier. In the coherent MTJs, the temperature dependence of the TMR ratios is mainly induced by the spin fluctuation at the ferromagnet/MgO interfaces and the spin-independent hopping within the MgO barrier.⁴¹ In the Heusler alloy-based MTJs, the spin fluctuation at the Heusler alloy/MgO interfaces may be the dominant cause to reduce the TMR ratios faster than the empirical law, possibly due to the formation of a small fraction of atomically disordered phases in the vicinity of the MgO barrier. The elimination of such disordered interfacial phases is critical to improve the TMR ratios at RT further to utilize the half-metallicity of the Heusler alloys. With such interfacial phases, the interfacial resonant states within the half-metallic bandgap are calculated to be formed at the half-metal/insulator interfaces under the presence of atomic mixing, breaking the half-metallicity.⁴² Here, the tunneling rate is slower than the spin-flip rate, resulting in the interfacial states for the minority spins to be effectively coupled to the metallic spin reservoir of the majority spin states.

Additionally, the spin polarization of a half-metallic Heusler alloy is calculated to be reduced significantly at temperatures much lower than their Curie temperatures even in a bulk form due to the change in hybridization by spin fluctuation.⁴³ The other theoretical calculations also revealed that an exchange stiffness constant can be reduced significantly at the interface between a Co-based Heusler alloy and a MgO barrier as

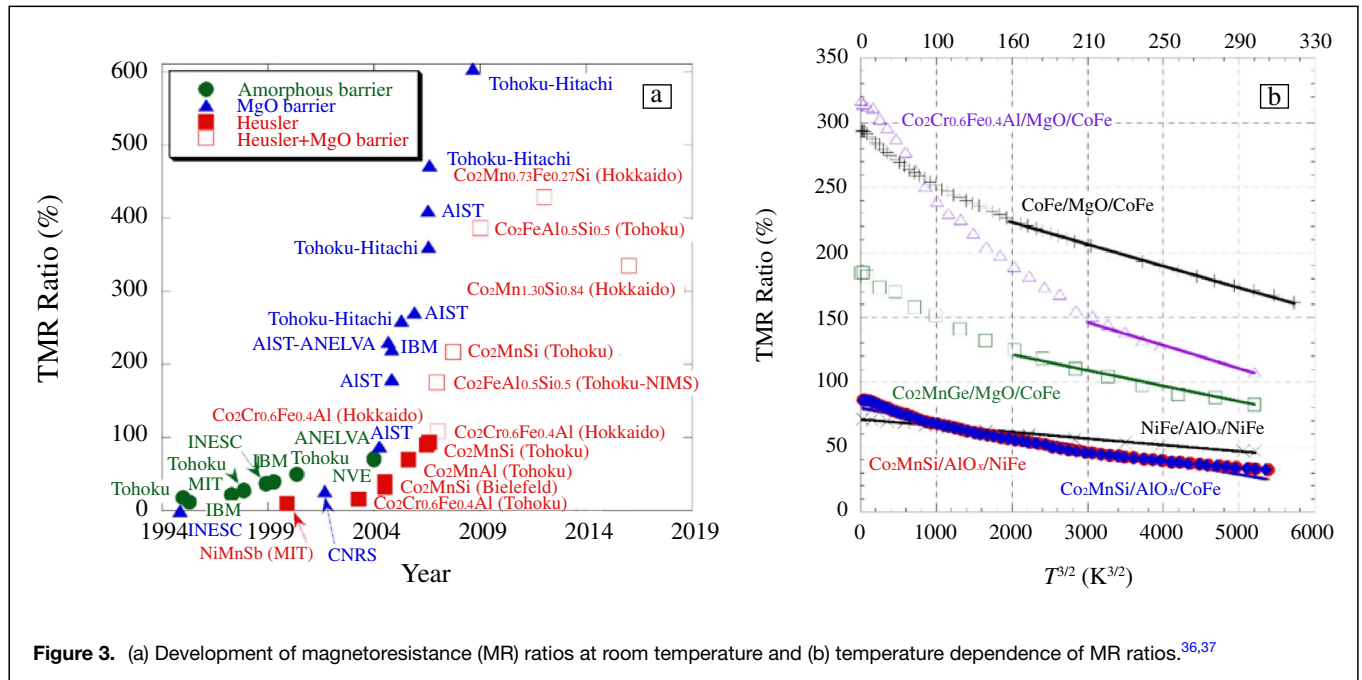


Figure 3. (a) Development of magnetoresistance (MR) ratios at room temperature and (b) temperature dependence of MR ratios.^{36,37}

compared with that in a bulk form due to the instability of the Co moment.⁴⁴ These conditions unique to a Heusler alloy-based MTJ can enhance the thermal fluctuation of spin moments in the Heusler alloy layer, inducing the large temperature dependence of a TMR ratio.⁴⁵ By eliminating such interfacial states, the temperature dependence of the TMR ratios can be minimized as observed for the conventional Al-O-based MTJs as shown in Figure 3b.

Magnetic anisotropy

A Heusler alloy typically has a cubic crystalline structure, which may not induce strong magnetic anisotropy. For the device implementation, however, perpendicular anisotropy needs to be induced by modifying the crystalline structures of the alloys or introducing interfacial coupling via a layer below, such as MgO and W. For the former structural modification, binary Heusler alloys in the tetragonal $D0_{22}$ -phase have been reported to induce perpendicular magnetic anisotropy.⁴¹ For example, ferrimagnetic Mn_3Ga has been reported to possess a large uniaxial anisotropy of 1×10^7 erg/cm³⁴⁶ and high Curie temperature of ~ 770 K.⁴⁷ Mn_3Ga MTJ has then been reported to show the TMR ratio of 40% at RT for $Mn_{0.62}Ga_{0.38}$ (30)/MgO (0.4)/MgO (1.8)/CoFeB (1.2) (thickness in nm).⁴⁸

For the latter interfacial coupling, similar to the Fe/MgO/Fe⁴⁹ and CoFeB/MgO/CoFeB systems,³² perpendicular anisotropy has been induced by attaching a MgO tunnel barrier to a Heusler alloy layer. For example, MTJ with Co_2FeAl (1)/MgO (1.8)/ $Co_{0.2}Fe_{0.6}B_{0.2}$ (1.4) (thickness in nm) was reported to exhibit a TMR ratio of 53% at RT.⁵⁰ By improving the interface with the insertion of a 0.1-nm-thick Fe ($Co_{0.5}Fe_{0.5}$) layer between the MgO and $Co_{0.2}Fe_{0.6}B_{0.2}$ layers, the TMR ratio was enhanced to 91% (82%), respectively. The corresponding RA is $1.31 \times 10^5 \Omega \cdot \mu m^2$. By further improving the MTJ quality, consisting of Co_2FeAl

(1.2)/MgO (1.8)/Fe (0.1)/CoFeB (1.3) (thickness in nm), TMR was improved to 132% with RA of $1 \times 10^6 \Omega \cdot \mu m^2$ at RT.⁵¹ Similar perpendicular anisotropy was induced with atomically smooth interfaces by substituting some of the Mg atoms with Al, forming $MgAl_2O_4$.⁵² The strong anisotropy at the interface is attributed to (1) the reduced in-plane magnetocrystalline anisotropy due to the lattice matching and (2) the promoted hybridization between Fe and O orbitals due to the Al redistribution near the interface.

Recently a body-centered-cubic (bcc) seed layer has been used to minimize the interfacial mixing with a fcc Heusler alloy layer.⁵³ For a bcc vanadium and tungsten seed layers, a strong (110) orientation in a Co-based Heusler alloy was reported in addition to the reduction in the crystallization temperature to the $B2$ phase at 335 K within 5 min. deposition time for 10–15-nm thick Heusler alloy film.⁵⁴ By implementing in a GMR junction, the GMR ratio of 0.03% at RT was reported for W (10)/ $Co_2FeAl_{0.5}Si_{0.5}$ (12.5)/W (1.2) or Ag (3)/ $Co_2FeAl_{0.5}Si_{0.5}$ (2.5) (thickness in nm). By optimizing the interfacial conditions further, larger perpendicular magnetic anisotropy and MR ratios can be induced.

Magnetic dynamics

For the improvement of data access time in magnetic memories to replace the level caches and temporary memories in the current CMOS-based computation, faster magnetization reversal needs to be achieved, requiring a ferromagnet with a low Gilbert damping constant α . α is an important parameter for the reduction of a switching current. To date, $Ni_{0.8}Fe_{0.2}$ has been used as a low damping material as shown in Figure 4. Among the conventional ferromagnets, $Co_{0.25}Fe_{0.75}$ has been reported to exhibit the smallest α of $(5 \pm 1.8) \times 10^{-4}$.⁵⁵ α can theoretically be proportional to the density of states (DOS) filled by electrons at the Fermi level.⁵⁶ This means the

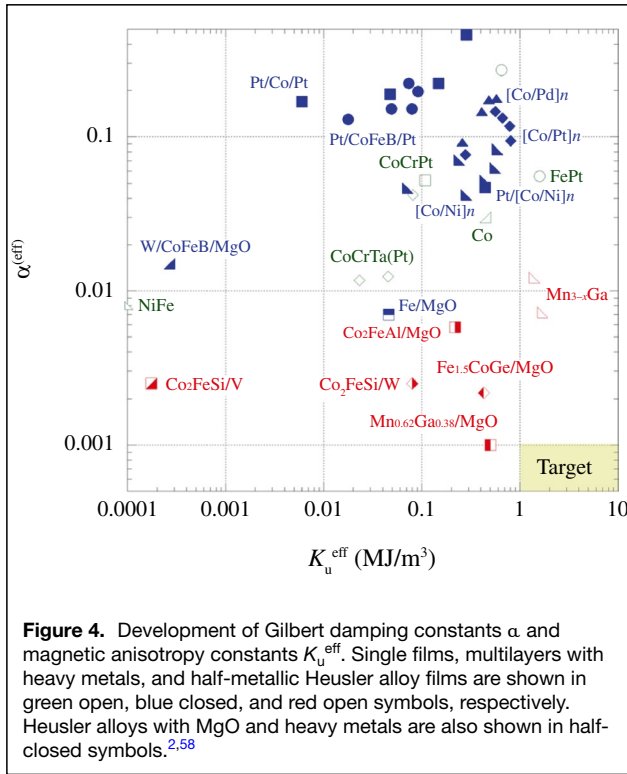


Figure 4. Development of Gilbert damping constants α and magnetic anisotropy constants K_u^{eff} . Single films, multilayers with heavy metals, and half-metallic Heusler alloy films are shown in green open, blue closed, and red open symbols, respectively. Heusler alloys with MgO and heavy metals are also shown in half-closed symbols.^{2,58}

half-metallic ferromagnets can be an ideal alternative for the improvement due to their limited number of DOS in nature. As shown in Figure 4, the Heusler alloys typically exhibit $\alpha < 0.01$. For example, α of 0.0005 was reported for Co_2MnSi and Co_2MnGe .⁵⁷ This can offer the corresponding relaxation time by almost two orders of magnitude better than that for NiFe, which is of the order of 10^8 s^{-1} .

For the integration of such spintronic devices, large perpendicular magnetic anisotropy is also essential.⁵⁸ For the conventional ferromagnets, FePt shows the largest $K_u^{\text{eff}} \sim 1.6 \times 10^7 \text{ erg/cm}^3$ but with large $\alpha \sim 0.06$. Heusler alloys, on the other hand, show similarly large $K_u^{\text{eff}} \sim 1.6 \times 10^7 \text{ erg/cm}^3$ and low $\alpha \sim 0.007$ for Mn-Ga alloys⁵⁹ and $K_u^{\text{eff}} \sim 4.3 \times 10^6 \text{ erg/cm}^3$ and lower $\alpha \sim 0.0022$ for $\text{Fe}_{1.5}\text{CoGe/MgO}$ bilayer.⁶⁰ Further development of Heusler alloys is required by controlling their spin-orbit coupling via atom substitution to achieve $\alpha < 0.001$ for a free ferromagnetic layer and $K_u^{\text{eff}} > 1.0 \times 10^7 \text{ erg/cm}^3$ for free and pinned ferromagnetic layers in next-generation magnetic storage and memory.

Spin-orbit torque

Spin Hall magnetoresistance

The spin Hall effect was predicted to induce the corresponding resistance changes with respect to the field (i.e., spin Hall magnetoresistance [SMR]).⁶¹ SMR was experimentally measured in $\text{Y}_3\text{Fe}_5\text{O}_{12}$ (YIG)/Pt bilayer.⁶² By using antiferromagnetic Heusler alloys, a large anomalous Hall effect⁶³ and a large θ_{SH} of $(5.3 \pm 2.4)\%$ was reported for Mn_3Sn .⁶⁴ This is due to a weak ferromagnetism induced in the noncollinear

antiferromagnetic alignment ($\sim 0.002 \mu_{\text{B}}/\text{Mn}$).⁶⁵ Such Heusler alloys were employed to develop an antiferromagnetic memory with the writing capability at THz frequency.⁶⁶ The SMR ratios are dependent on the spin Hall angles θ_{SH} , which is listed in Figure 5. For Mn_3Sn , θ_{SH} is reported to be $(5.3 \pm 2.4)\%$ with the spin diffusion length of $(0.75 \pm 0.67) \text{ nm}$ at RT.⁶⁴ Currently, θ_{SH} for the Heusler alloys are almost one order of magnitude smaller than those for heavy metals, for example, -35 (-50%) for W⁶⁷ (WO_x)⁶⁸ and 5.6% for Pt.⁶⁹ Further search for new Heusler alloys is essential for the SOT-based device applications.

Spin caloritronics

SOT also induces spin caloritronic effects, such as spin Seebeck and Nernst effects (SSE and SNE, respectively). A spin current was originally generated under thermal gradient formed in $\text{Ni}_{0.8}\text{Fe}_{0.2}/\text{Pt}$.⁷³ For SSE and SNE, the figure of merit ZT can be determined as⁷³

$$ZT(\text{SSE}) = \frac{\sigma S^2}{\kappa} T, \quad 3$$

$$ZT(\text{SNE}) = \frac{\sigma N^2}{\kappa} T, \quad 4$$

where T : temperature, σ : electrical conductivity, S : Seebeck coefficient, N : the Nernst coefficient and κ : thermal conductivity. Here, $ZT > 1$ is needed for practical device applications. ANE is normally proportional to the intrinsic magnetization of the material. For $\text{Cr}_2\text{O}_3/\text{Pt}$, a Nernst signal of $\sim 0.015 \mu\text{V/K}$ was reported at RT⁷⁴ as shown in Figure 5. For a Mn_3Sn Heusler alloy, a larger Nernst coefficient of $\sim 0.35 \mu\text{V/K}$ was reported.⁷⁰ This increase is due to the fact that the transverse thermoelectric conductivity is determined by the Berry curvature in the vicinity of the Fermi level, while the anomalous Hall conductivity is defined as the sum of the Berry curvature for all the occupied bands. Accordingly, a Weyl metal can be advantageous for spin caloritronic applications due to the unique Berry curvature at Weyl points near the Fermi level.

Summary and future perspectives

As shown in the roadmap for Heusler alloys,⁷⁵ the ultimate goal of spintronic devices using the alloy is to develop those with all Heusler alloys, including ferromagnetic, nonmagnetic, insulating, and antiferromagnetic Heusler alloys. Such a device can eliminate any issues of interfacial spin fluctuation due to the mismatching between these layers. The spintronics industry has been entered to a challenging time for the development of new technologies and devices, including energy-assisted magnetic recording and fourth-generation MRAM. These require new materials, especially Heusler alloys with the half-metallic nature. For the former device, a ferromagnetic Heusler alloy with large magnetic anisotropy with low damping constants is required to achieve fast magnetization

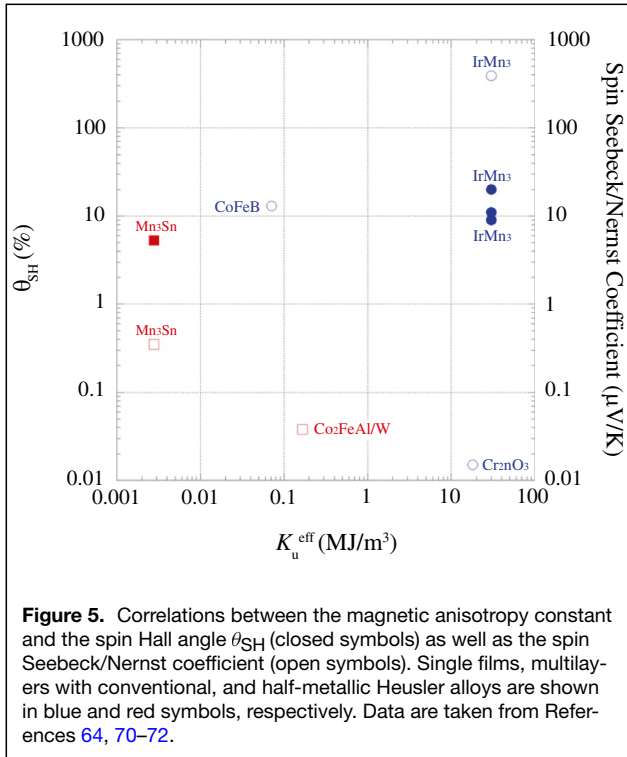


Figure 5. Correlations between the magnetic anisotropy constant and the spin Hall angle θ_{SH} (closed symbols) as well as the spin Seebeck/Nernst coefficient (open symbols). Single films, multilayers with conventional, and half-metallic Heusler alloys are shown in blue and red symbols, respectively. Data are taken from References 64, 70–72.

reversal in a free layer of a MR junction. For the latter, a ferromagnetic Heusler alloy with large SOT and/or voltage controllability of magnetic anisotropy is needed for low-energy magnetization reversal. These new technologies with new Heusler alloys can also be used for unconventional computing, such as stochastic and neuromorphic computation, as well as highly sensitive magnetic sensors, including medical imaging. Additional energy harvesting with spin caloritronics⁷⁶ can be achieved using an antiferromagnetic Heusler alloy. These new Heusler alloys have been developed by materials search with machine learning in combination with first-principles calculations,^{77–80} the details of which can be found in “Data approaches for materials discovery” written by Wolverton et al.⁸¹ in this issue of *MRS Bulletin*.

Acknowledgments

The authors would like to thank the financial support by EPSRC Grant Nos. (EP/I000933/1, EP/K03278X/1, EP/M02458X/1, and EP/V007211/1), JST CREST (Grant No. JPMJCR17J5), and JST-EC DG RTD Coordinated research project (Grant No. FP7-NMP3-SL-2013-604398).

Conflict of interest

The authors confirm there is no conflict of interest.

Open Access

This article is licensed under a Creative Commons Attribution 4.0 International License, which permits use, sharing,

adaptation, distribution and reproduction in any medium or format, as long as you give appropriate credit to the original author(s) and the source, provide a link to the Creative Commons license, and indicate if changes were made. The images or other third party material in this article are included in the article’s Creative Commons license, unless indicated otherwise in a credit line to the material. If material is not included in the article’s Creative Commons license and your intended use is not permitted by statutory regulation or exceeds the permitted use, you will need to obtain permission directly from the copyright holder. To view a copy of this license, visit <http://creativecommons.org/licenses/by/4.0/>.

References

1. A. Hirohata, K. Takanashi, *J. Phys. D* **47**, 193001 (2014)
2. A. Hirohata, K. Yamada, Y. Nakatani, L. Prejbeanu, B. Diény, P. Pirro, B. Hillebrands, *J. Magn. Magn. Mater.* **509**, 166711 (2020)
3. B. Diény, I.L. Prejbeanu, K. Garello, P. Gambardella, P. Freitas, R. Lehndorff, W. Raberg, U. Ebels, S.O. Demokritov, J. Akerman, A. Deac, P. Pirro, C. Adelmann, A. Anane, A.V. Chumak, A. Hirohata, S. Mangin, S.O. Valenzuela, M. Cengiz Onbasli, M. d’Aquino, G. Prenat, G. Finocchio, L. Lopez-Diaz, R. Chantrell, O. Chubykalo-Fesenko, P. Bortolotti, *Nat. Electron.* **3**, 446 (2020)
4. A. Hirohata, W. Frost, S. Fukami, in *Nanomagnetic Materials: Fabrication, Characterization and Application*, ed by A. Yamaguchi, A. Hirohata, B.J.H. Stadler (Elsevier, Amsterdam, 2021), pp. 1–10
5. J. Slonczewski, *J. Magn. Magn. Mater.* **159**, L1 (1996)
6. L. Berger, *Phys. Rev. B* **54**, 9353 (1996)
7. R.A. de Groot, F.M. Mueller, P.G. van Engen, K.H.J. Buschow, *Phys. Rev. Lett.* **50**, 2024 (1983)
8. N.F. Mott, H.S.W. Massey, *The Theory of Atomic Collisions*, 3rd ed. (Oxford University Press, Oxford, 1965)
9. J. Sinova, I. Žutić, *Nat. Mater.* **11**, 368 (2012)
10. M.N. Baibich, J.M. Broto, A. Fert, F. Nguyen Van Dau, F. Petroff, P. Etienne, G. Creuzet, A. Friederich, J. Chazelas, *Phys. Rev. Lett.* **61**, 2472 (1988)
11. G. Binasch, P. Grünberg, F. Saurenbach, W. Zinn, *Phys. Rev. B* **39**, 4828(R) (1989)
12. M. Jullière, *Phys. Lett. A* **54**, 225 (1975)
13. M. Hayashi, L. Thomas, C. Rettner, R. Moriya, X. Jiang, S.S.P. Parkin, *Phys. Rev. Lett.* **97**, 207205 (2006)
14. W. Jiang, P. Upadhyaya, W. Zhang, G. Yu, M.B. Jungfleisch, F.Y. Fradin, J.E. Pearson, Y. Tserkovnyak, K.L. Wang, O. Heinonen, S.G.E. te Velthuis, A. Hoffmann, *Science* **349**, 283 (2015)
15. P.A.M. Dirac, *The Principles of Quantum Mechanics*, 4th ed. (Oxford University Press, Oxford, 1958)
16. M.I. Dyakonov, V.I. Perel, *Phys. Lett. A* **35**, 459 (1971)
17. J.E. Hirsch, *Phys. Rev. Lett.* **83**, 1834 (1999)
18. Y.K. Kato, R.C. Myers, A.C. Gossard, D.D. Awschalom, *Science* **306**, 1910 (2004)
19. I. Dzyaloshinskii, *J. Phys. Chem. Solids* **4**, 241 (1958)
20. T. Moriya, *Phys. Rev.* **120**, 91 (1960)
21. M. Morota, Y. Niimi, K. Ohnishi, D.H. Wei, T. Tanaka, H. Kontani, T. Kimura, Y. Otani, *Phys. Rev. B* **83**, 174405 (2011)
22. N. Reynolds, P. Jadaun, J.T. Heron, C.L. Jermain, J. Gibbons, R. Collette, R.A. Buhrman, D.G. Schlom, D.C. Ralph, *Phys. Rev. B* **95**, 064412 (2017)
23. S. Mühlbauer, B. Binz, F. Jonietz, C. Pfleiderer, A. Rosch, A. Neubauer, R. Georgii, P. Böni, *Science* **323**, 915 (2009)
24. S. Datta, B. Das, *Appl. Phys. Lett.* **56**, 665 (1990)
25. R. Ramaswamy, J.M. Lee, K. Cai, H. Yang, *Appl. Phys. Rev.* **5**, 031107 (2018)
26. J.W. Jung, Y. Sakuraba, T.T. Sasaki, Y. Miura, K. Hono, *Appl. Phys. Lett.* **108**, 102408 (2016)
27. S. Ikeda, J. Hayakawa, Y. Ashizawa, Y.M. Lee, K. Miura, H. Hasegawa, M. Tsunoda, F. Matsukura, H. Ohno, *Appl. Phys. Lett.* **93**, 082508 (2008)
28. W.H. Butler, X.-G. Zhang, T.C. Schulthess, J.M. MacLaren, *Phys. Rev. B* **63**, 054416 (2001)
29. J. Mathon, A. Umerski, *Phys. Rev. B* **63**, 220403(R) (2001)
30. S.S.P. Parkin, C. Kaiser, A. Panchkula, P.M. Rice, B. Hughes, M. Samant, S.-H. Yang, *Nat. Mater.* **3**, 862 (2004)
31. S. Yuasa, T. Nagahama, A. Fukushima, Y. Suzuki, K. Ando, *Nat. Mater.* **3**, 868 (2004)
32. S. Ikeda, K. Miura, H. Yamamoto, K. Mizunuma, H.D. Gan, M. Endo, S. Kanai, J. Hayakawa, F. Matsukura, H. Ohno, *Nat. Mater.* **9**, 721 (2010)
33. T. Scheike, H. Sukegawa, K. Inomata, T. Ohkubo, K. Hono, S. Mitani, *Appl. Phys. Express* **9**, 053004 (2016)

34. N. Tezuka, N. Ikeda, F. Mitsuhashi, S. Sugimoto, *Appl. Phys. Lett.* **94**, 162504 (2009)
35. Z. Wen, H. Sukegawa, S. Kasai, K. Inomata, S. Mitani, *Phys. Rev. Appl.* **2**, 024009 (2014)
36. A. Hirohata, Y. Otani, in *Epitaxial Ferromagnetic Films and Spintronic Applications*, ed by A. Hirohata, Y. Otani (Research Signpost, Kerala, 2009), pp. 224–225
37. K. Elphick, W. Frost, M. Samiepour, T. Kubota, K. Takanashi, H. Sukegawa, S. Mitani, A. Hirohata, *Sci. Technol. Adv. Mater.* **22**, 235 (2020)
38. H.-X. Liu, Y. Honda, T. Taira, K. Matsuda, M. Arita, T. Uemura, M. Yamamoto, *Appl. Phys. Lett.* **101**, 132418 (2012)
39. C.H. Shang, J. Nowak, R. Jansen, J.S. Moodera, *Phys. Rev. B* **58**, R2917 (1998)
40. H. Schneider, G. Jakob, M. Kallmayer, H.-J. Elmers, M. Cinchetti, B. Balke, S. Wurmehl, C. Felser, M. Aeschlimann, H. Adrian, *Phys. Rev. B* **74**, 174426 (2006)
41. K. Elphick, K. Yoshida, T. Roy, T. Ichinose, K. Kunimatsu, T. Tsuchiya, K. Z. Suzuki, M. Tsujikawa, Y. Nagai, S. Mizukami, M. Shirai, A. Hirohata, *Condens. Matter Mater. Sci.* (2020). <https://arxiv.org/abs/2010.04493>
42. P. Mavropoulos, M. Ležaić, S. Blügel, *Phys. Rev. B* **72**, 174428 (2005)
43. M. Ležaić, Ph. Mavropoulos, J. Enkovaara, G. Bihlmayer, S. Blügel, *Phys. Rev. Lett.* **97**, 026404 (2006)
44. A. Sakuma, Y. Toga, H. Tsuchiura, *J. Appl. Phys.* **105**, 07C910 (2009)
45. Y. Miura, K. Abe, M. Shirai, *Phys. Rev. B* **83**, 214411 (2011)
46. H.-W. Bang, W. Yoo, Y. Choi, C.-Y. You, J.-L. Hong, J. Dolinšek, M.-H. Jung, *Curr. Appl. Phys.* **16**, 63 (2016)
47. J. Winterlik, B. Balke, G.H. Fecher, C. Felser, M.C.M. Alves, F. Bernardi, J. Morais, *Phys. Rev. B* **77**, 054406 (2008)
48. Q.L. Ma, T. Kubota, S. Mizukami, X.M. Zhang, H. Naganuma, M. Oogane, Y. Ando, T. Miyazaki, *Appl. Phys. Lett.* **101**, 032402 (2012)
49. A. Manchon, C. Ducruet, L. Lombard, S. Auffret, B. Rodmacq, B. Dieny, S. Pizzini, J. Vogel, V. Uhlir, M. Hochstrasser, G. Panaccione, *J. Appl. Phys.* **104**, 043914 (2008)
50. Z. Wen, H. Sukegawa, S. Kasai, M. Hayashi, S. Mitani, K. Inomata, *Appl. Phys. Express* **5**, 063003 (2012)
51. Z. Wen, H. Sukegawa, T. Furubayashi, J. Koo, K. Inomata, S. Mitani, J.P. Hadorn, T. Ohkubo, K. Hono, *Adv. Mater.* **26**, 6483 (2014)
52. J.P. Hadorn, H. Sukegawa, T. Ohkubo, S. Mitani, K. Hono, *Acta Mater.* **145**, 306 (2018)
53. W. Frost, A. Hirohata, *IEEE Trans. Magn.* **52**, 4400604 (2016)
54. W. Frost, M. Samiepour, A. Hirohata, *J. Magn. Magn. Mater.* **484**, 100 (2019)
55. M.A.W. Schoen, D. Thonig, M.L. Schneider, T.J. Silva, H.T. Nembach, O. Eriksson, O. Karis, J.M. Shaw, *Nat. Phys.* **12**, 839 (2016)
56. V. Kambarsky, *Can. J. Phys.* **48**, 2906 (1970)
57. C. Guillemard, S. Petit-Watelot, L. Pasquier, D. Pierre, J. Ghanbaja, J.C. Rojas-Sánchez, A. Bataille, J. Rault, P. Le Fèvre, F. Bertran, S. Andrieu, *Phys. Rev. Appl.* **11**, 064009 (2019)
58. E.Y. Vedmedenko, R. Kawakami, D. Sheka, P. Gambardella, A. Kirilyuk, A. Hirohata, C. Binek, O. Chubykalo-Fesenko, S. Sanvito, B.J. Kirby, J. Grollier, K. Everschor-Sitte, T. Kampfrath, C.Y. You, A. Berger, *J. Phys. D* **53**, 453001 (2020)
59. H. Naganuma, G. Kim, Y. Kawada, N. Inami, K. Hatakeyama, S. Iihama, K.M.N. Islam, M. Oogane, S. Mizukami, Y. Ando, *Nano Lett.* **15**, 623 (2015)
60. A. Conca, A. Niesen, G. Reiss, B. Hillebrands, *AIP Adv.* **9**, 085205 (2019)
61. M.I. Dyakonov, *Phys. Rev. Lett.* **99**, 126601 (2007)
62. H. Nakayama, M. Althammer, Y.T. Chen, K. Uchida, Y. Kajiwara, D. Kikuchi, T. Ohtani, S. Geprags, M. Opel, S. Takahashi, R. Gross, G.E.W. Bauer, S.T. Goennenwein, E. Saitoh, *Phys. Rev. Lett.* **110**, 206601 (2013)
63. S. Nakatsuji, N. Kiyohara, T. Higo, *Nature* **527**, 212 (2015)
64. P.K. Muduli, T. Higo, T. Nishikawa, D. Qu, H. Isshiki, K. Kondou, D. Nishio-Hamane, S. Nakatsuji, Y. Otani, *Phys. Rev. B* **99**, 184425 (2019)
65. S. Tomiyoshi, Y. Yamaguchi, *J. Phys. Soc. Jpn.* **51**, 2478 (1982)
66. K. Olejnik, T. Seifert, Z. Kašpar, V. Novák, P. Wadley, R.P. Campion, M. Baumgartner, P. Gambardella, P. Němec, J. Wunderlich, J. Sinova, P. Kužel, M. Müller, T. Kampfrath, T. Jungwirth, *Sci. Adv.* **4**, 3566 (2018)
67. C.F. Pai, L. Liu, Y. Li, H.W. Tseng, D.C. Ralph, R.A. Buhrman, *Appl. Phys. Lett.* **101**, 122404 (2012)
68. K.-U. Demasius, T. Phung, W. Zhang, B.P. Hughes, S.-H. Yang, A. Kellock, W. Han, A. Pushp, S.S.P. Parkin, *Nat. Commun.* **7**, 10644 (2016)
69. J.-C. Rojas-Sánchez, N. Reyren, P. Laczkowski, W. Saverio, J.-P. Attané, C. Deranlot, M. Jamet, J.-M. George, L. Vila, H. Jaffrès, *Phys. Rev. Lett.* **112**, 106602 (2014)
70. M. Mizuguchi, S. Nakatsuji, *Sci. Technol. Adv. Mater.* **20**, 262 (2019)
71. W. Zhang, W. Han, S.-H. Yang, Y. Sun, Y. Zhang, B. Yan, S.S.P. Parkin, *Sci. Adv.* **2**, e1600759 (2016)
72. R. Thompson, J. Ryu, G. Choi, S. Karube, M. Kohda, J. Nitta, B.-G. Park, *Phys. Rev. Appl.* **15**, 014055 (2021)
73. K. Uchida, S. Takahashi, K. Harii, J. Ieda, W. Koshibae, K. Ando, S. Maekawa, E. Saitoh, *Nature* **455**, 778 (2008)
74. S. Seki, T. Ideue, M. Kubota, Y. Kozuka, R. Takagi, M. Nakamura, Y. Kaneko, M. Kawasaki, Y. Tokura, *Phys. Rev. Lett.* **115**, 266601 (2015)
75. A. Hirohata, H. Sukegawa, H. Yanagihara, I. Žutić, T. Seki, S. Mizukami, R. Swaminathan, *IEEE Trans. Magn.* **51**, 0800511 (2015)
76. S.M. Wu, W. Zhang, K.C. Amit, P. Borisov, J.E. Pearson, J.S. Jiang, D. Lederman, A. Hoffmann, A. Bhattacharya, *Phys. Rev. Lett.* **116**, 097204 (2016)
77. The University of Alabama, Heusler Database. <http://heusleralloys.mint.ua.edu/>
78. A.O. Olynyk, E. Antono, T.D. Sparks, L. Ghadbeigi, M.W. Gaultois, B. Meredig, A. Mar, *Chem. Mater.* **28**, 7324 (2016)
79. S. Sanvito, C. Oses, J. Xue, A. Tiwari, M. Zic, T. Archer, P. Tozman, M. Venkatesan, M. Coey, S. Curtarolo, *Sci. Adv.* **3**, e1602241 (2017)
80. F. Legrain, J. Carrete, A. van Rookeghem, G.K.H. Madsen, N. Mingo, *J. Phys. Chem. B* **122**, 625 (2017)
81. C. Wolverton, J. He, K. Rabe, *MRS Bull.* **47**(6), (2022) □



Atsufumi Hirohata received his BSc and MSc degrees in physics from Keio University, Japan, in 1995 and 1997, respectively, and his PhD degree in physics from the University of Cambridge, UK, in 2001. From 2001 to 2002, he was a postdoctoral associate in the Cavendish Laboratory at the University of Cambridge. He moved to the Francis Bitter Magnet Laboratory at the Massachusetts Institute of Technology in 2002 as a postdoctoral associate. He then became a researcher in the Department of Materials at Tohoku University, Japan, in 2003 and at the Frontier Research System at RIKEN, Japan, in 2005. Hirohata became a lecturer in the Department of Electronics (now Department of Electronic Engineering) at the University of York in 2007, and was promoted to a reader, professor, and senior professor in 2011, 2014, and 2017, respectively. He edited three books and published more than 160 articles and 35 inventions. His research interests include spintronics and magnetic materials. Hirohata can be reached by email at atsufumi.hirohata@york.ac.uk.



David C. Lloyd received his MPhys degree in 2013, MSc degree in 2015, and PhD degree in 2019 in physics from the University of York, UK. For two years (2019–2020), he worked at the Okinawa Institute of Science and Technology Graduate University, Japan, as a postdoctoral fellow. In 2021, he returned to the UK as a postdoctoral research associate at the University of York. His research interests include *in situ* electron microscopy, characterization of nanoscale materials, and the growth of functional magnetic materials. Lloyd can be reached by email at david.lloyd@york.ac.uk.